ORIGINAL ARTICLE



Geochemical modeling to aid experimental design for multiple isotope tracer studies of coupled dissolution and precipitation reaction kinetics

Mingkun Chen^{1,2} · Peng Lu^{1,3} · Yongchen Song² · Chen Zhu¹

Received: 25 September 2023/Revised: 24 October 2023/Accepted: 27 October 2023 © The Author(s), under exclusive licence to Science Press and Institute of Geochemistry, CAS and Springer-Verlag GmbH Germany, part of Springer Nature 2023

Abstract It is a challenge to make thorough but efficient experimental designs for the coupled mineral dissolution and precipitation studies in a multi-mineral system, because it is difficult to speculate the best experimental duration, optimal sampling schedule, effects of different experimental conditions, and how to maximize the experimental outputs prior to the actual experiments. Geochemical modeling is an efficient and effective tool to assist the experimental design by virtually running all scenarios of interest for the studied system and predicting the experimental outcomes. Here we demonstrated an example of geochemical modeling assisted experimental design of coupled labradorite dissolution and calcite and clayey mineral precipitation using multiple isotope tracers. In this study, labradorite (plagioclase) was chosen as the reactant because it is both a major component and one of the most reactive minerals in basalt. Following our isotope doping studies of single minerals in the last ten years, initial solutions in the simulations were doped with multiple isotopes (e.g., Ca and Si). Geochemical modeling results show that the use of isotope tracers gives us orders of magnitude more sensitivity than the conventional method based on concentrations and allows us to decouple dissolution and precipitation reactions at near-equilibrium condition. The simulations suggest that the precise unidirectional dissolution rates can inform us which rate laws plagioclase dissolution has followed. Calcite precipitation occurred at near-equilibrium and the multiple isotope tracer experiments would provide near-equilibrium precipitation rates, which was a challenge for the conventional concentration-based experiments. In addition, whether the precipitation of clayey phases is the rate-limiting step in some multi-mineral systems will be revealed. Overall, the modeling results of multimineral reaction kinetics will improve the understanding of the coupled dissolution-precipitation in the multi-mineral systems and the quality of geochemical modeling prediction of CO₂ removal and storage efficacy in the basalt systems.

Keywords Kinetics · Feldspar · Isotope doping · Near-equilibrium · CO₂ sequestration · Basalt

Mingkun Chen mc83@iu.edu

Peng Lu peng.lu@aramco.com

Yongchen Song songyc@dlut.edu.cn

Published online: 21 December 2023

- Department of Earth and Atmospheric Sciences, Indiana University, Bloomington, IN 47405, USA
- School of Energy and Power Engineering, Dalian University of Technology, Dalian 116024, China
- ³ EXPEC Advanced Research Center, Saudi Aramco, 31311 Dhahran, Saudi Arabia

1 Introduction

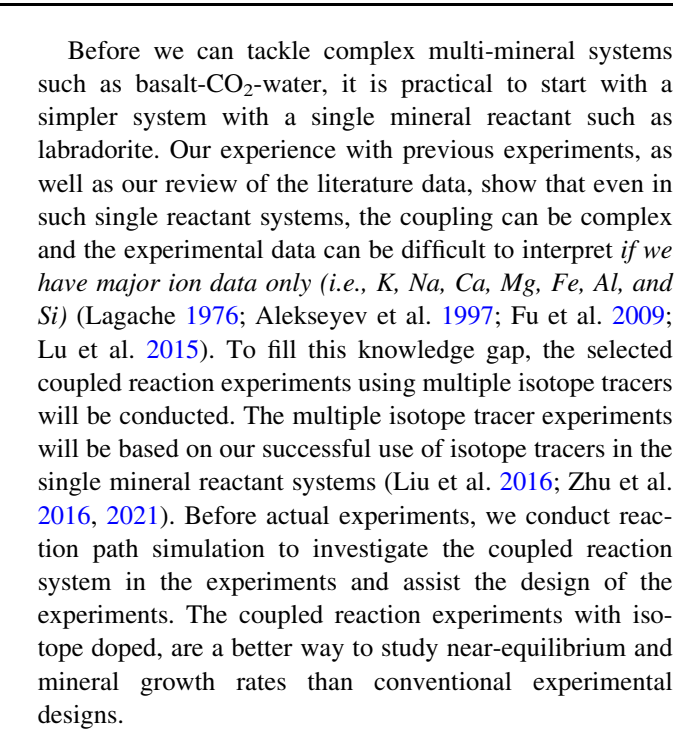
CO₂ storage in mafic/ultramafic rock reservoirs such as basalt and olivine is an efficient strategy for mitigating anthropogenic carbon emissions through in-situ geochemical reactions (Xiong and Giammar 2014; Raza et al. 2022; Chen et al. 2023). Our current knowledge of geochemical kinetics is largely based on single mineral dissolution rates far from equilibrium such as the kinetics parameter databases by U.S. Geological Survey (Palandri and Kharaka 2004), Marini (Marini 2007), CO₂CRC (Black et al. 2015),



French Geological Survey (Marty et al. 2015) and French National Centre for Scientific Research (CNRS) (Heřmanská et al. 2022, 2023). Only a limited amount of nearequilibrium reaction rate and precipitation rate data are available (Taylor et al. 2000; Schott et al. 2009). However, the systems that store CO₂, e.g., soils and aquifers, are multi-mineral systems, and the aqueous solutions are predominantly near-equilibrium with respect to the participating minerals (Drever 1997). In short, there is a lack of experimental data on the near-equilibrium, multi-mineral kinetics of such systems (Schott et al. 2009; Zhu et al. 2020, 2021).

Because of the lack of relevant data, most current geochemical models use far-from-equilibrium dissolution rate constants and assume their validity under near-equilibrium conditions for dissolution through ad hoc assumptions of rate laws (Zhu et al. 2020). Moreover, these studies also assume that the same extrapolations can be extended to precipitation reactions. The uncertainties in these models are propagated when the geochemical model part is coupled with transport processes (diffusion, dispersion, and advection) in coupled reactive transport models (RTM) (Steefel and MacQuarrie 1996; Steefel et al. 2015; Li et al. 2017), which are applied to CO₂ storage in aquifers and soils (Dai et al. 2020). Although such studies provide useful insights (Liu et al. 2011; Zhang et al. 2016; Lu et al. 2022), it is still prudent and valuable, for the sake of contributing to the implementation of climate change mitigation strategies, to investigate the geochemical kinetics at near-equilibrium.

Experimental, field, and modeling evidence shows that, in a multi-mineral system, the overall reaction rate in the system is determined by the coupling of dissolution and precipitation reactions (Alekseyev et al. 1997; Zhu 2005; Maher et al. 2009). The coupling processes can be complex. Zhu et al. hypothesized that the coupling of reactions brings the reacting solutions close to equilibrium with respect to feldspars, which reduces the feldspar dissolution rates via the chemical affinity term in the rate laws and contributes to the apparent discrepancy between lab and field rates (Zhu et al. 2004). Daval et al. (2010) showed the reduction of diopside dissolution rates at conditions of near-equilibrium increases the time needed to reach a complete carbonation reaction by a six-fold factor compared to the TST (Transition State Theory)-based rates. For the basalt-CO₂-water system, it has been speculated that the slow precipitation of (Ca, Fe, Mg) clay and carbonate minerals could reduce the dissolution rates of the basalt glass and (Ca, Mg, Fe) primary silicates over time (Gysi and Stefánsson 2012). The overall reactivity in plagioclaserich compositions can be reduced with the coating of precipitates (clay minerals and iron oxide) on the reactants (Gadikota et al. 2020).



2 Background and hypotheses

Here we just briefly introduce the necessary background of reaction kinetics. Following the convention, near-equilibrium is defined as the region of $\Delta_r G/RT > -5$ (Burch et al. 1993; Rimstidt 2014), although this definition has the flaw that $\Delta_r G$ values are related to how the chemical formula for the mineral of interest is written.

For the labradorite dissolution, we can write the reaction

$$Na_{0.4}Ca_{0.6}Al_{1.6}Si_{2.4}O_8+3.2H_2O$$

 $\rightarrow 0.4Na^++0.6Ca^{2+}+1.6Al(OH)_4^-+2.4SiO_2(aq)$ (1)

The rates of labradorite dissolution by convention are based on Si flux,

$$r_{\text{net}} = r_{+} - r_{-} = \frac{1}{v \cdot S_{A}} \frac{d[SiO_{2}]}{dt}$$
 (2)

where r_+ and r_- denote the forward and reverse reaction rates (mol labradorite m⁻² s⁻¹) defined in Table 1, respectively. The net reaction rate r_{net} (mol m⁻² s⁻¹) is also often called the overall rate. v stands for the stoichiometric coefficient of Si in the silicate mineral of interest, e.g., 2.4 for labradorite. S_A (m²/L) stands for the reactive surface area (Helgeson et al. 1984) or the concentration of the reactive surface sites (Stumm 1992). However, in practice, these properties are currently inaccessible, and S_A is approximated by either the Braunauer-Emmett-Teller (BET) (Brunauer et al. 1938) or geometric surface area (Lasaga 1998).



Theoretically, when a system approaches equilibrium, the thermodynamic drive diminishes, and the net reaction rate decreases. r_{net} is a function of $\Delta_{\text{r}}G$ for an *elementary* reaction in accordance with the *Principle of Detailed* Balance if the forward and reverse reactions have the same mechanisms (Ohlin et al. 2009; Liu et al. 2016),

$$r_{\text{net}} = r_{+} - r_{-} = r_{+} \left(1 - e^{\Delta_{\text{r}} G/RT} \right)$$
 (3)

If Eq. (3) holds, r_+ should be independent of $\Delta_r G$; r_- rises exponentially in the near-equilibrium region; $r_{\rm net}$ has a "plateau" at the far-from-equilibrium region but decreases exponentially when the experimental solutions approach equilibrium with respect to labradorite (Fig. 1). At equilibrium, $r_{\rm net} = 0$. In the far-from-equilibrium region, the reverse reaction is negligible, $r_{\rm net} = r_+$. However, in the near-equilibrium region, the reverse reaction is no longer negligible. The conventional experimental method based on [Si] measures $r_{\rm net}$. The effects of the diminishing thermodynamic drive are expressed as reduced net dissolution rates as the system approaches equilibrium.

For albite dissolution from far-from-equilibrium to near-equilibrium, Burch et al. investigated the steady-state dissolution rates of albite in aqueous solutions at 80 °C and pH 8.8 as a function of solution saturation state expressing by the sum of the rates of two parallel reactions (Burch et al. 1993),

$$r_{\text{net}} = k_1 \left(1 - \left(e^{-n\left(\frac{|\Delta_{\Gamma}G|}{RT}\right)^{m_1}} \right) \right) + k_2 \left(1 - \left(e^{-\frac{|\Delta_{\Gamma}G|}{RT}} \right) \right)^{m_2} \tag{4}$$

where k_1 and k_2 denote the rate constants in units of mol m⁻² s⁻¹, and n, m_1 , and m_2 are empirical parameters fitted from the experimental data (Zhu 2009). Taylor et al. (2000) used the empirical rate law from Burch et al. (1993) to interpret their experiments of labradorite dissolution at

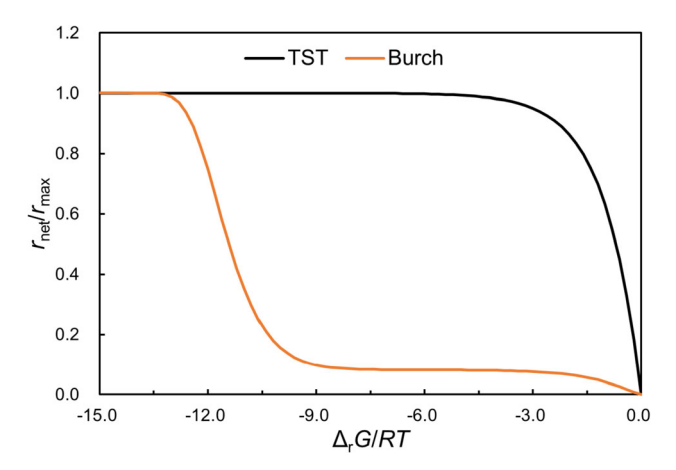


Fig. 1 A schematic graph to illustrate the differences among normalized net rates $(r_{\rm net}/r_{\rm max})$ as described by Eqs. (3) and (4). TST stands for "transition state theory" rate law and Burch stands for the the sum of the rates of two parallel reactions experimentally derived from Burch et al. (1993)

25 °C and pH 3.2. Equation (4) suggests two parallel mechanisms that operate separately under far-from-equilibrium and near-equilibrium conditions, respectively (Burch et al. 1993; Hellmann and Tisserand 2006). Under far-from-equilibrium condition, dissolution is driven by the nucleation at dislocation outcrops of etch pits that are the source of steps across the surface. Closer to equilibrium and below a critical Gibbs free energy value $\Delta G_{\rm crit}$, etch pits stop nucleating, and dissolution occurs only at pre-existing edges and corners at a much lower rate and becomes more uniform across the crystal surface (Taylor et al. 2000).

The dissolution of labradorite could lead to the precipitation of secondary phases (e.g., calcite and clay minerals) (Carroll and Knauss 2005). To simplify the system, we choose allophane (amorphous silica) to represent all clay precipitation containing Si and Al.

$$Ca^{2+} + HCO_3^- \rightarrow CaCO_3(s) + H^+$$
 (5)

$$\begin{array}{c} 2\text{Al}(\text{OH})_{4}^{-} + 1.22\text{SiO}_{2}(\text{aq}) \rightarrow 2\text{OH}^{-} + 0.5\text{H}_{2}\text{O} + (\text{Al}_{2}\text{O}_{3}) \\ & \cdot (\text{SiO}_{2})_{1.22} \cdot (\text{H}_{2}\text{O})_{2.50}(\text{am}) \end{array}$$

(6)

$$SiO_2(aq) \rightarrow SiO_2(s)$$
 (7)

When the Si-bearing secondary phase precipitates, the conventional experimental method based on the concentration analysis measures the apparent net rate ($\stackrel{\sim}{r}_{\rm net}$) rather than the "true" net rate ($r_{\rm net}$):

$$\hat{r}_{\text{net}} = r_{+} - r_{-} - r_{\text{2nd}} \tag{8}$$

where $r_{2\mathrm{nd}}$ is the rate sum of Si-containing secondary phases such as allophane and chalcedony. Almost all the rate data available in the literature at near-equilibrium are the apparent net rate $\widetilde{r}_{\mathrm{net}}$, unless it could be verified that no Si-containing secondary phases were precipitated. However, it is a broad challenge to verify possible secondary phase precipitation. The same challenge exists for the mass balance analysis from Ca perspective when calcite precipitates.

Generally, the TST-derived rate equation has been used for modeling mineral precipitation with parameters obtained from far-from-equilibrium dissolution rate experiments (Palandri and Kharaka 2004; Marty et al. 2015). For modeling secondary carbonate mineral growth, the BCF (Burton, Cabrera, and Frank) equation is recommended for net precipitation due to better representation with the non-linear part of the BCF model (Burton et al. 1951; Pham et al. 2011),

$$r_{\text{net}} = k_{\text{BCF}} (1 - \Omega)^2 \tag{9}$$

where $k_{\rm BCF}$ is the rate constant that could be calculated using the same way as the TST model in order to explain



the effect of different affinity terms, and Ω is the saturation ratio (IAP/K_{sp}). According to the BCF crystal growth theory (Burton et al. 1951), n = 2 stands for spiral growth of screw dislocation.

The labradorite dissolution and secondary mineral precipitation reactions can be coupled. The overall reaction can be written as

```
\label{eq:Labradorite} \begin{split} Labradorite + 2.2 H_2O + 0.6 HCO_3^- &\rightarrow 0.4 Na^+ + (1.424 - x) SiO_2(aq) \\ + OH^- + 0.6 Calcite + x Chalcedony + 0.8 Allophane \end{split}
```

(10)

However, how these reactions are coupled is still unknown. We intend to conduct reaction path modeling to illustrate the possible coupled scenarios and to design experiments to test the following hypotheses about reaction coupling.

Hypothesis 1 The isotope-doped experiments will generate unidirectional rates of labradorite dissolution from far-from-equilibrium to near-equilibrium with higher precision and accuracy. Whether labradorite dissolution follows TST or Burch-type rate law will be discernable.

Our previous study showed Si isotope tracer experiments provide unidirectional rates of feldspar dissolution (r_+) (Zhu et al. 2020). r_+ is constant across solution saturation states if the reaction mechanism or reactive surface area does not change. In contrast, if r_+ decreases dramatically from far-from-equilibrium to near-equilibrium, it indicates the reaction mechanism switch occurs. In this study, we designed the multi-isotope doped experiments aided by reaction path modeling to measure $\tilde{r}_{\rm net}$ directly. This constitutes a more direct test of the dissolution mechanism hypothesis.

Hypothesis 2 The coupled dissolution and precipitation experiments will generate calcite precipitation rates at near-equilibrium, which is still measurable with isotope ratios.

There are few calcite growth experiments near calcite equilibrium (Xu et al. 2010). During our coupled reaction modeling, the chemical compositions of the initial solution are saturated with respect to calcite, thus labradorite dissolution and calcite precipitation occur simultaneously. Calcite precipitation rates at near-equilibrium can be calculated directly based on the Ca mass balance equation, which is aided by the unidirectional labradorite (Ca contributor) dissolution rate based on the ²⁹Si/²⁸Si ratios.

Hypothesis 3 Calcite precipitation is so fast that simulation results show no difference whether to assume local equilibrium or kinetics or different rate laws in the models. Because only a few experimental precipitation rates are available, the precipitation kinetic model is often extended from the dissolution model with the assumption of the *Principle of Detailed Balance* (Liu et al. 2016). At near-equilibrium condition, calcite maybe in local equilibrium with the aqueous solution, indicating that calcite precipitation is fast enough. For this coupled experiments and modeling based on a single mineral reactant, we could explain the effect of different affinity term-based rate laws on calcite precipitation.

3 Experimental and modeling designs

3.1 Multiple isotope tracer experimental design

We designed the multi-isotope doped experiments with a single reactant labradorite, one of the major crystalline mineral phases of basalt (Gudbrandsson et al. 2011; Wolff-Boenisch et al. 2011). In order to model the batch reaction experiments in the laboratory, the parameters of the initial solution of Experiment C were simplified from the conditions of the CarbFix project (Snæbjörnsdóttir et al. 2017) where CO₂ was injected into the basalt reservoir. The injected fluid of Phase I of the CarbFix project has a pH of 3.85 and dissolved inorganic carbon (DIC) of 0.823 mol/ kgw. The calculated log P_{CO2} ranges from -4 to -2and the temperature range is 20-50 °C. Our models are designed to mimic these conditions. The temperature of 60 °C was selected to expedite the reaction progress. The stabilized pH is around 8.5 in the reservoir away from the injection well for the CarbFix project (Galeczka et al. 2022). Reaction path modeling of in-situ mineralization of CO₂ at the CarbFix site indicates that zeolites and smectites will start to form at high pH (Snæbjörnsdóttir et al. 2018).

The preparation of the isotope-doped initial solutions follows our earlier works (Zhu et al. 2016, 2020, 2021). The initial solution is prepared by dissolving a certain amount of KHCO₃ and CaCl₂. ²⁹Si and ⁴³Ca stock solutions are added into the initial solution to form the isotope difference between the labradorite solid and the aqueous solution. The dissolution rates of labradorite (Si and Ca release rate) are therefore defined. The amounts of KHCO₃, CaCl₂, ²⁹SiO₂ stock solution, ⁴³CaCl₂ stock solution, and DI water are recorded. In order to ensure that pH is 8.5 at 60 °C, the solution pH is rapidly adjusted to 7.0 at 22 °C to avoid CO₂ loss by adding a small amount of HCl or KOH. According to the results of equilibrium modeling, the initial solution is adjusted to the equilibrium with calcite using CaCl₂. 0.4500 (\pm 0.001) g of labradorite and 45 g (i.e., ~ 45 mL) initial solution are mixed in a 50-mL polypropylene bottle to initiate mineral dissolution. 0.0045 g calcite powders (53–105 µm) are added to each bottle as



Table 1 List of symbols and definitions

Symbol	Definition
$\Delta_{ m r} G$	Gibbs free energy of the reaction (kJ/mol)
k	The apparent rate constant of reaction in mol m ⁻² s ⁻¹
Ω	The saturation ratio $(IAP/K_{\rm sp})$
IAP	The ion activity product
$K_{\rm sp}$	Equilibrium constant
R	Gas constant $(8.314 \text{ J mol}^{-1} \text{ K}^{-1})$
$r_{\rm net}$	The net or overall reaction rate in mol m ⁻² s ⁻¹ ; $r_{\text{net}} = r_+ - r$
$\stackrel{\sim}{r}_{ m net}$	Apparent net rate in mol m ⁻² s ⁻¹ . $\tilde{r}_{\text{net}} = r_+ - r r_{2\text{nd}}$
r_+	The dissolution rate of labradorite dissolution in mol m ⁻² s ⁻¹
r'_+	The dissolution rate of labradorite dissolution in mol L ⁻¹ s ⁻¹ ; $r'_{+}S_A$
<i>r</i> _	Reverse rate of labradorite dissolution reaction (precipitation or formation) in mol m ⁻² s ⁻¹ ; similarly, for r'_{-}
r_{2nd}	Precipitation rate of secondary mineral in mol m ⁻² s ⁻¹ ; similarly, for r'_{2nd}
$r'_{\rm pre}$	$r'_{\text{pre}} = vr'_{-} + r'_{2\text{nd}}$, defined as "precipitation rate" in mol L ⁻¹ s ⁻¹
$r'_{\text{pre,Si}}$	The total Si-containing phase precipitation rate measured in Si (mol Si L ⁻¹ s ⁻¹)
S_A	Surface area load of feldspar (m ² /L) in the reactor; $S_A = s_A * m/V$, where m denotes the mass (g) of reactant, V the volume of solution in the reactor, and s_A the specific surface area (m ² /g)
T	Temperature (K)
t	Time (s)
Δt	Time interval from time t to time $t + 1$
V	The volume of the solution in a reactor (L)
[X]	The total concentration of element or species X
$[X]^t$	The total concentration of element or species X at time t
v	The stoichiometric coefficient in the molecular formula of mineral
Abbrevio	ations
Lab	Labradorite
Cal	Calcite
Allo	Allophane
Cha	Chalcedony
am	Amorphous
aq	Aqueous species
pre	Precipitation
max	Maximum value
SI	Saturation index

seeds to facilitate the calcite growth. The bottles are sealed with plastic wrap and heated to 60 ± 0.5 °C using a water bath for the duration of the experiment. In addition, we designed Experiment D to explain the effect of activity ratio $[\text{Ca}^{2+}]/[\text{CO}_3^{2-}]$ and low HCO_3^- on the coupled system. The initial solution parameters for the two experiments are summarized in Table 2.

3.2 Interpretation of experimental data

After the experiments, the solutions are filtered with 0.22 mm nitrocellulose membrane filter paper. The concentrations of K, Ca, Si, Al, and Na are analyzed by ICP-OES.

The alkalinity is measured using an auto-titrator by HCl titration. The Si and Ca isotope ratios are measured using high-resolution multiple-collector inductively coupled plasma mass spectrometry (MC-ICP-MS). It is noted that all solution samples for measuring Si isotopes will be purified by cation exchange chromatography to reduce the disturbance from other cations (Georg et al. 2006). BET surface areas of labradorite and calcite seeds are measured via low pressure N_2 adsorption measurement before the experiments (Thommes et al. 2015).

As we described in the background, $\stackrel{\sim}{r}_{\rm net}$ can be calculated based on the evolution of Si and Ca concentrations. Our previous work shows that the dissolution rate r_+ can be



Table 2 Chemical composition of the initial solutions

Experiment Condition	C	D
Temperature (°C)	60	60
pН	8.5	8.5
Total Ca (μM)	11.15	68.58
⁴³ Ca(μM)	5.00	0.06
Total K (mM)	823.0	1.569
Total C (mM)	823.0	1.569
Total Si (29Si, mM)	0.1000	0.1000
Total Cl (mM)	0.0223	0.1372
Act[Ca ²⁺]/Act [CO ₃ ²⁻]	1.0E-5	1.0

measured while Si precipitation occurs (Zhu et al. 2016). The unidirectional dissolution rate for labradorite can be derived from Si and Ca mass balance with the aid of Si and Ca isotope ratios. Details about the calculation procedure are described in our previous studies (Zhu et al. 2016, 2021). It is noted that Si and Ca isotope fractionation due to dissolution and precipitation are negligible (Zhu et al. 2016; Harrison et al. 2023). The unidirectional dissolution rates (r_+) are best fitted by solving the mass balance equations for Si concentrations and Si isotopes for any time interval from t to t+1 assuming the rates of labradorite dissolution and secondary mineral precipitation are constant,

$$[Si]^{t+1} = \left(v_{Si}r'_{+} - r'_{pre,Si}\right)\Delta t + [Si]^{t}$$

$$[^{28}Si]^{t+1} = \left(v_{Si}f_{28,lab}r'_{+} - f_{28,t}r'_{pre,Si}\right)[Si]^{t}\Delta t + f_{28,t}[^{28}Si]^{t}$$

$$[^{29}Si]^{t+1} = \left(v_{Si}f_{29,lab}r'_{+} - f_{29,t}r'_{pre,Si}\right)[Si]^{t}\Delta t + f_{29,t}[^{29}Si]^{t}$$

$$(11)$$

where the only unknowns are the dissolution rate r'_{+} and precipitation rate of the Si-containing phase $r'_{\text{pre,Si}}$, r'_{+} and $r'_{\text{pre,Si}}$ are defined in Table 1. Here, we choose ²⁸Si and ²⁹Si mass equations to dissolve it.

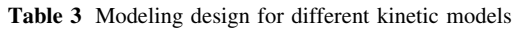
For Ca concentrations and Ca isotopes, the calculation procedure is conducted using the same way:

$$[Ca]^{t+1} = (v_{Ca}r'_{+} - r'_{cal})\Delta t + [Ca]^{t}$$

$$[^{42}Ca]^{t+1} = (v_{Ca}f_{42,lab}r'_{+} - f_{42,t}r'_{cal})[Ca]^{t}\Delta t + f_{42,t}[^{42}Ca]^{t}$$

$$[^{43}Ca]^{t+1} = (v_{Ca}f_{43,lab}r'_{+} - f_{43,t}r'_{cal})[Ca]^{t}\Delta t + f_{43,t}[^{43}Ca]^{t}$$
(12)

where the only unknowns are the dissolution rate r'_+ and the calcite precipitation rate r'_{Cal} . It is possible to determine the Ca and Si derived unidirectional dissolution rates of labradorite. In addition, the calcite precipitation rate r'_{Cal} can be calculated based on the Si-derived unidirectional dissolution rate, even if the variation of Ca isotope could not be detected.



Model	Labradorite	Calcite	Chalcedony	Allophane
C0	TST	TST	TST	TST
C1	Burch	TST		
C2	TST	Equilibrium		
C3	TST	BCF		
C4	TST	TST	Equilibrium	Equilibrium
D0	TST	TST	TST	TST
D1	Burch	TST		
D2	TST	Equilibrium		
D3	TST	BCF		
D4	TST	TST	Equilibrium	Equilibrium

3.3 Reaction path modeling

To investigate the coupled reaction process and test the validity of experimental designs, reaction path simulations were calculated with the software PHREEQC 3.6.4 (Parkhurst and Appelo 2013) and the database *EWR_Mafic.dat* developed by our team. The general rate equation based on the transition state theory (TST) was given (Lasaga 1981),

$$r_{net} = S_A * k_{r} * (1 - \Omega^p)^q$$

$$= S_A * \left(\sum_{k} A_k e^{-E_{a,k}} \prod_{i} a_{i,j}^{n_i} \right) * (1 - \Omega^p)^q$$
(13)

where k_r is the rate constant, A_k is the Arrhenius pre-exponential factor (mol m⁻² s⁻¹), E_a is the activation energy (J mol⁻¹), T is the temperature (K), R is the gas constant, a_i is the aqueous species activity, the exponent's n_i represents the reaction order with respect to species a_i , Ω is the saturation ratio (IAP/K_{sp}), and p and q are the empirical parameters describing the saturation dependence.

The simulations were divided into two series of batch simulations based on the experimental design (Experiment C and D) including Model C and Model D, respectively (Table 3). The concentrations of solutes reported from the experimental design (Table 2) were used for the initial solution of the input file. The amount of dissolved and precipitated phases and the chemical compositions of the aqueous solution were calculated. Kinetic model parameters describing the dissolution and precipitation rates are summarized in Table 4. The base cases Model C0 and D0 use the TST rate laws for all the primary and secondary minerals. The local equilibrium models for calcite (Model C2 and D2) and chalcedony and allophane (Model C4 and D4) were built to explore the effect of local equilibrium. Meanwhile, the corresponding mineral seeds (0.001 mol) were introduced for local equilibrium to maintain the saturation state.



Table 4 Kinetic parameters describing the dissolution and precipitation rates in the reaction path calculations

Mineral	Acid mechanism		Neutral mechanism		Base mechanism		Empirical		Ref		
	$A_a \text{ mol/} $ (m^2s)	E _{a,a} kJ/mol	n_a	$A_b \text{ mol/} $ (m^2s)	E _{a,b} kJ/mol	$A_c \text{ mol/} $ (m^2s)	E _{a,c} kJ/mol	n_c	p	q	
Labradorite	5.89×10^3	58.0	1.0	0.17	60.0	1.50×10^{-5}	50.0	- 0.35	0.42	1.00	Heřmanská et al. (2022)
Calcite ¹				6.59×10^{4}	66.0	1.04×10^{9}	67.0	1.63	0.50	2.00	Marty et al. (2015)
Chalcedony ²				1.85×10^{-1}	68.7				1.00	1.00	Palandri and Kharaka (2004)
Allophane ³	2.56×10^{-1}	43.0	0.51	5.00×10^{-5}	38.0	2.87	46.0	0.58	1.00	1.00	Zhang et al. (2019)
Kaolinite	2.56×10^{-4}	43.0	0.51	5.00×10^{-8}	38.0	2.87×10^{-3}	46.0	0.58	1.00	1.00	Marty et al. (2015)

¹[HCO₃⁻] is used for the calcite kinetic model instead of [OH⁻]. Only considering calcite precipitation

Different kinetic dissolution models were used for labradorite in Model C1 and D1 to evaluate the effect of dissolution mechanism switch from far-from-equilibrium to near-equilibrium. The kinetic formula from Taylor et al. (2000) showed the non-convergence and unstable properties, resulting in the interruption of model running. Therefore, we choose the rate law formula from Burch et al. (1993) for labradorite to account for these two parallel mechanisms, due to the similar pH of the experiments in Burch et al. (1993) and this study. The affinity term from the albite research was used (Eq. (8), $k_1/k_2 = 11.2$, $n = 8.40 \times 10^{-17}$, $m_1 = 15$, $m_2 = 1.45$), however, the rate constant k_1 was calculated using the same calculated values with that of Model C0 and D0. In addition, we also conducted Model C3 and D3 to explain the effects of different affinity terms with calcite on the coupled reaction. These different kinetic models or local equilibrium can be easily implemented with minor modifications in the data block of input files.

In order to illustrate the evolution of isotope during the coupled reaction process, we calculated the isotope concentration and ratio based on the incremental dissolution and precipitation amount in the modeling results. The mass balance equations for isotope Si and Ca are extended from Eqs. (11) and (12):

$$\begin{bmatrix} {}^{i}Si \end{bmatrix}^{t} = \begin{bmatrix} {}^{i}Si \end{bmatrix}^{t-1} + 2.4 \times f_{i,Lab} \times d_{Lab}^{t-1} - 1.0 \times f_{i}^{t-1} \\
\times d_{Cha}^{t-1} - 1.22 \times f_{i}^{t-1} \times d_{Allo}^{t-1}$$
(14)

$${[}^{j}\text{Ca}{]}^{t} = {[}^{j}\text{Ca}{]}^{t-1} + 0.6 \times f_{i,\text{Lab}} \times d_{\text{Lab}}^{t-1} - 1.0 \times f_{i}^{t-1} \times d_{\text{Cal}}^{t-1}$$
(15)

where i = 28, 29 and 30, j = 40, 42, 43 and 44, and the natural abundance of Si and Ca refers to the previous study (Berglund and Wieser 2011).

4 Modeling results

4.1 Effects of different rate laws for labradorite

Figure 2 showed distinct differences between the modeling results from Model C0 using TST dissolution kinetics for labradorite and Model C1 based on the Bruch model. For Model C0, Si and Na concentrations increased due to labradorite dissolution, while Ca concentration kept constant due to the coupled labradorite dissolution-calcite precipitation. After about 5 days, the Al concentration slightly decreased, indicating the precipitation of the secondary phase sinks more Al than the release amount from labradorite dissolution. The saturation index of labradorite increased from -5.5 to -1.0 during the first 5 days and approached 0 for the remaining reaction periods, indicating the labradorite dissolution varied from far-from-equilibrium to near-equilibrium. The aqueous solution was supersaturated with respect to allophane and near-equilibrium for chalcedony. However, no chalcedony precipitation occurred. The amount of calcite precipitation increased continuously while the saturation index of calcite was always about 0.002, which indicates that calcite precipitation occurred at near equilibrium. Due to the slower labradorite dissolution kinetics of the Burch model (Model C1) than that of TST-based Model C0, the amounts of labradorite dissolution and calcite and allophane precipitation were dramatically smaller in Model C1 than those in Model C0 (Fig. 1c).

The concentration variations of ions were not large enough to distinguish considering the measurement error and uncertainty. However, Fig. 2d showed the evolution of Si isotope ratios for Model C0 and C1 were significantly different and the differences are measurable. Due to the



²Amorphous silica is used for chalcedony

 $^{^{3}}$ Rate law of allophane is adopted from the kaolinite rate law formulation and the rate constant of allophane (- 11.05) is about 3 orders of magnitude higher than that of kaolinite (- 13.96) (Ralston 2018)

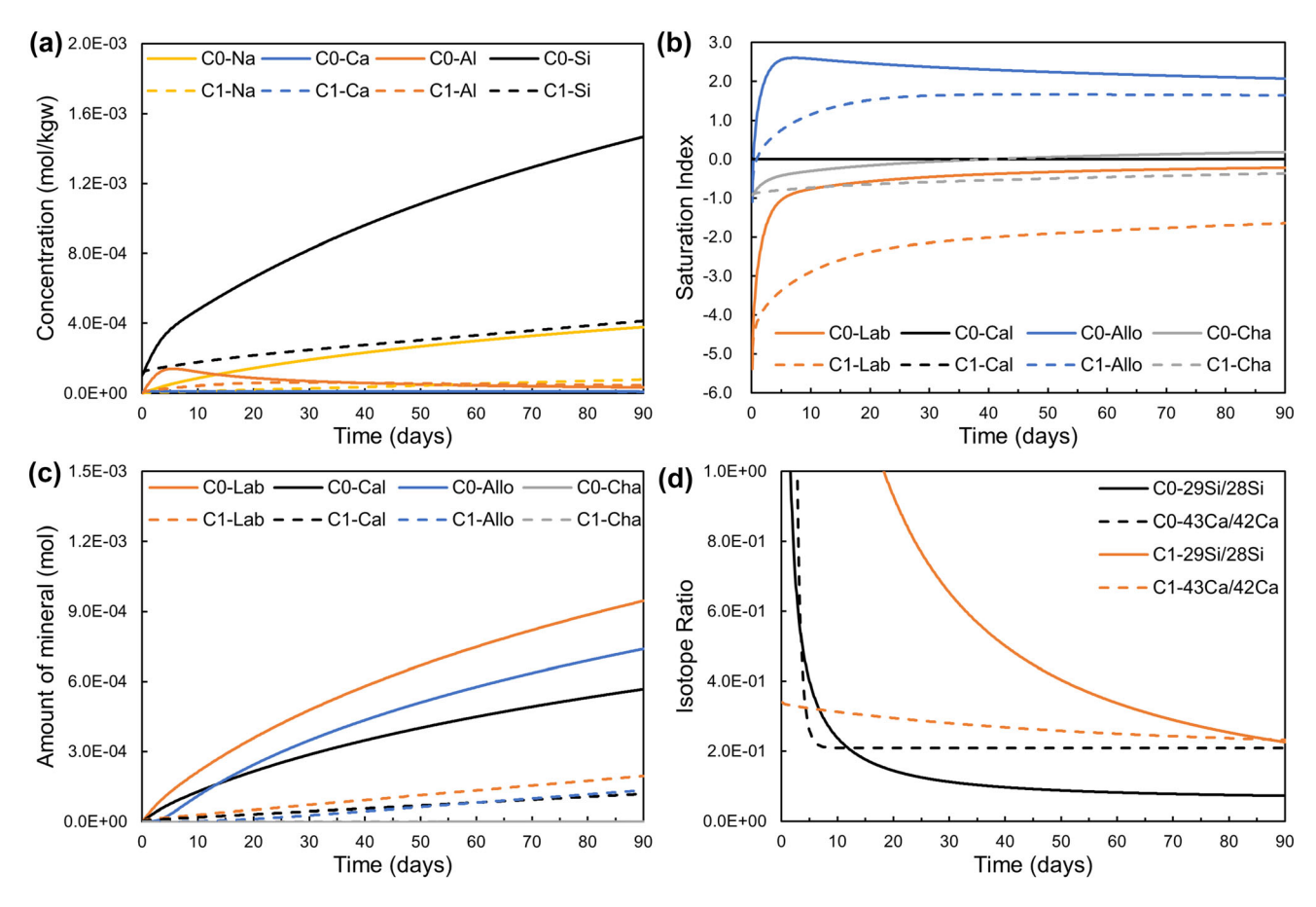


Fig. 2 Temporal evolution of solution chemistry and isotopes from different labradorite dissolution kinetic models [TST (C0) and Burch (C1)] for Model C. **a** Concentrations of aqueous species. **b** Saturation indexes of minerals. **c** Amount of labradorite dissolution and secondary precipitation. **d** Isotope ratios of Si (²⁹Si/²⁸Si) and Ca (⁴³Ca/⁴²Ca). The abbreviation of minerals refers to Table 1

faster dissolution of labradorite using the TST rate law, more Si and Ca were released from the labradorite for Model C0 than those for Model C1. Therefore, Si and Ca isotope ratios (²⁹Si/²⁸Si) and Ca (⁴³Ca/⁴²Ca) decreased faster for Model C0, especially Ca isotope ratios decreased sharply and then remained constant after 10 days. The unidirectional dissolution rate of labradorite can be derived from the Si isotope ratios and Si concentration based on mass balance Eq. (11). The effect of Si isotope fractionation can be ignored, because the errors in rate determinaresulting from Si isotope fractionation are $<\pm 0.04\%$ (Zhu et al. 2016). Therefore, the modeling results suggested the isotope-doped experimental design allows the acquisition of unidirectional rates of labradorite dissolution from far-from-equilibrium to near-equilibrium with high precision and accuracy, which can in turn inform which rate laws that plagioclase dissolution has followed.

The calcite precipitation equation shows that the calcite precipitation rate constant depends on the bicarbonate concentration (Eq. 5) and Table 4). With a lower concentration of HCO₃⁻ and the activity ratio [Ca²⁺]/[CO₃²⁻] approaching 1.0, Model D0 and D1 show lower reaction

rates and mass transfer amounts compared with Model C0 and C1 in Figs. 3. Figure 3b demonstrated the aqueous solutions in the coupled system stayed very close to equilibrium with respect to labradorite after 0.2 days and 10 days for Model D0 and D1, respectively. Labradorite continued to dissolve, and the secondary phases (calcite and allophane) continued to precipitate until all labradorites were exhausted. In short, if the labradorite dissolution followed the Burch rate law, the mass transfer rate of the coupled reaction system would decrease at least one order of magnitude regardless of the initial conditions from Model C and D. This indicates the coupled system is labradorite dissolution controlled.

4.2 Calcite precipitation rates at near-equilibrium

Labradorite dissolution and calcite precipitation reactions are coupled via the common element Ca in the system. Figures 2b and 3b showed calcite precipitation occurred at near-equilibrium with respect to calcite, whose saturation index was almost zero for Model C0 and D0. The weight percentages and concentrations of labradorite and



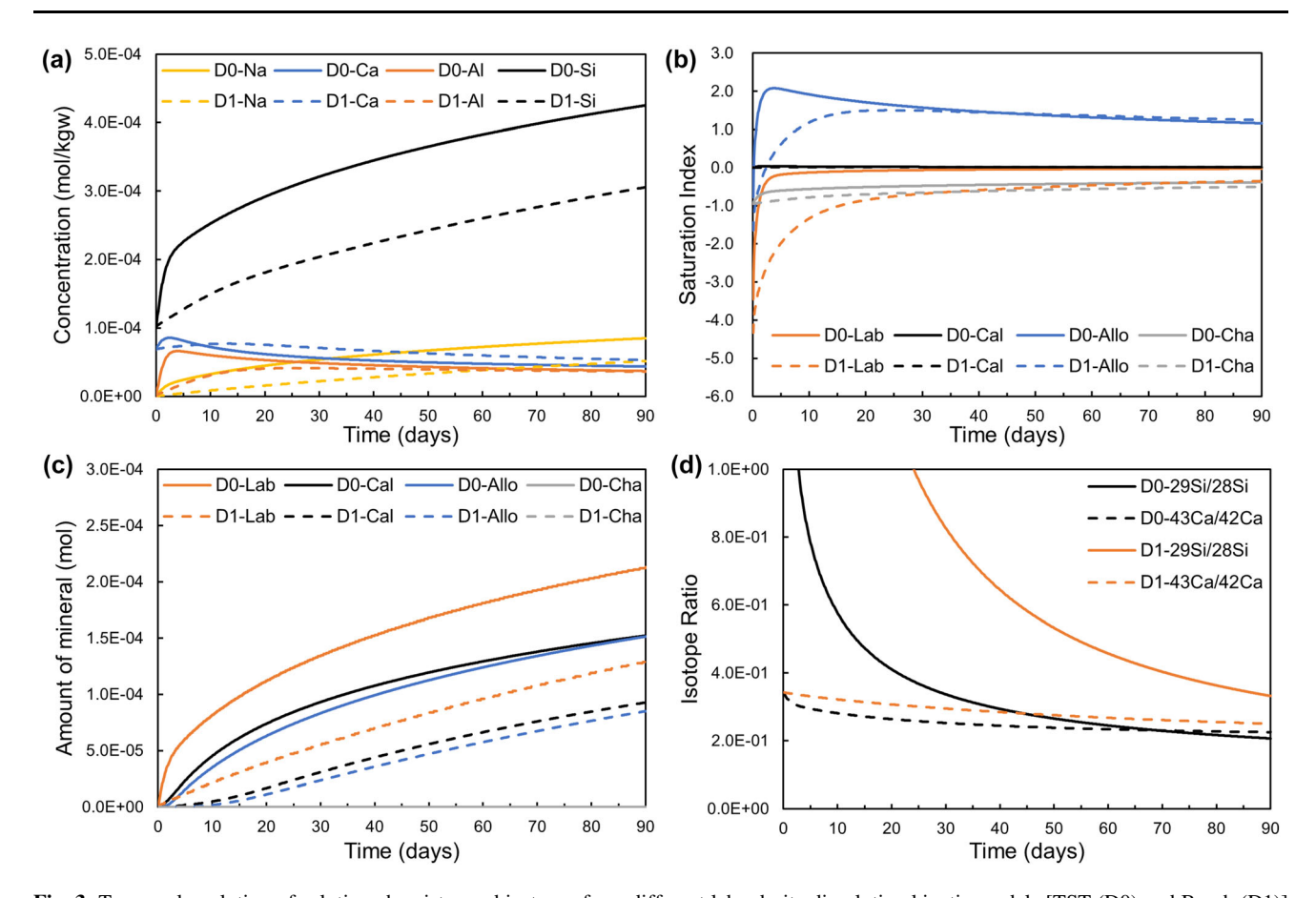


Fig. 3 Temporal evolution of solution chemistry and isotopes from different labradorite dissolution kinetic models [TST (D0) and Burch (D1)] for Model D. **a** Concentrations of aqueous species. **b** Saturation indexes of minerals. **c** Amount of labradorite dissolution and secondary precipitation. **d** Isotope ratios of Si (29Si/28Si) and Ca (43Ca/42Ca). The abbreviation of minerals refers to Table 1

Table 5 Weight percentages and concentrations of labradorite and secondary precipitations before and after reaction

_	Mod	el C0	Mod	del D0	
Time	0 days	90 days	0 days	90 days	
Labradorite, mol/kgw	0.03680	0.03586	0.03680	0.03659	
Calcite, mol/kgw	0.0009999	0.001567	0.0009999	0.001152	
Allophane, mol/kgw	0	0.0007392	0	0.0001515	
Labradorite, wt%	99.0103	96.8238	99.0103	98.5267	
Calcite, wt%	0.9897	1.5584	0.9897	1.1426	
Allophane, wt%	0.0000	1.6178	0.0000	0.3307	
Sum	100.0	100.00	100.0	100.0	

secondary precipitations were calculated shown in Table 5. After 90 days, approximately 0.01g and 0.003g labradorite was dissolved for Model C0 and D0. Meanwhile, > 1.0 wt% calcite and allophane precipitated except for allophane at Model D0, which is enough for the quantitative analysis of minerals based on XRD spectra. In addition, the precipitation could be detected only when the weight percentage > 0.1%. The simulation results showed that Ca concentrations decreased little or nearly constant for Model C0 and D0 in Fig. 4. The conventional experimental method (i.e., only measuring time-series Ca concentrations) would fail to determine calcite precipitation rates in

such situations. However, Fig. 4 showed Si and Ca isotope ratios are much more sensitive than Si and Ca concentrations, respectively. Therefore, we can deduce the calcite precipitation rates at near-equilibrium condition based on the differences between the Ca isotope ratio-based Ca release rate from labradorite dissolution and observed Ca concentrations in the solution.

When the variations of Ca isotope ratios are not detectably large, the unidirectional labradorite dissolution rate with time can be calculated based on the temporal evolution of Si isotope ratios if Si and Ca have the proportional release rates from labradorite dissolution. The assumption



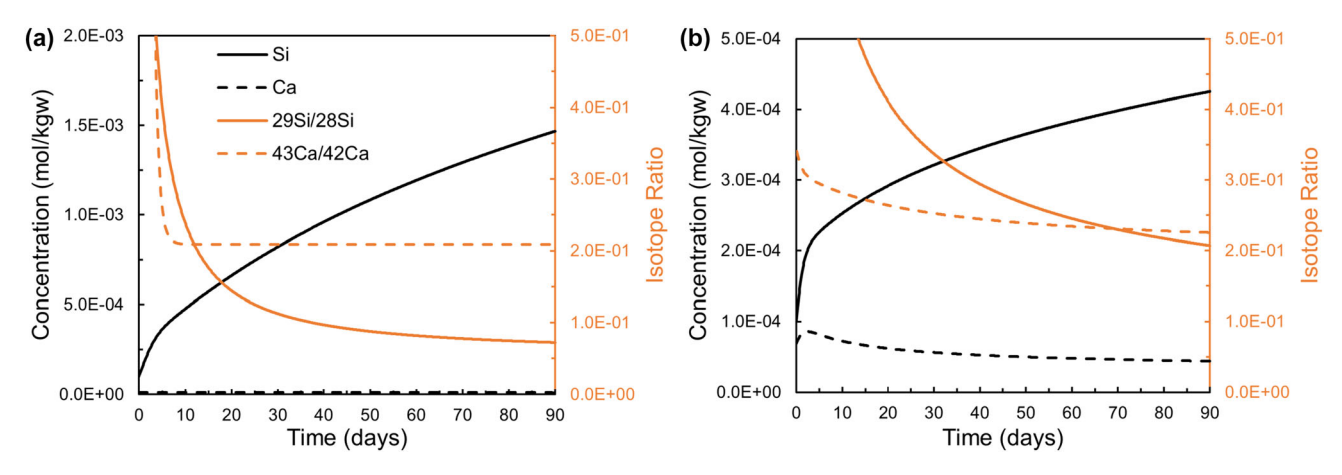


Fig. 4 Temporal evolution of Si and Ca concentrations and isotope ratios of Model C0 (a) and Model D0 (b). Calcite precipitation rates at near-equilibrium can be calculated based on Ca mass balance equation, which is aided by the Ca release rate from labradorite dissolution based on the ²⁹Si/²⁸Si ratios. The abbreviation of mineral names refers to Table 1

is that the dissolution of labradorite is stoichiometric after a steady state of dissolution is achieved, meaning that there are 2.4 mol Si and 0.6 mol Ca released for 1 mol labradorite dissolution. Therefore, calcite precipitation rates at near-equilibrium can be calculated based on the Ca mass balance equation, which is aided by the labradorite dissolution based on the $^{29}\text{Si}/^{28}\text{Si}$ ratio. We will test this assumption with experimental data. Previous experimental results showed $\Delta^{44/42}\text{Ca} = -0.02\%$ for Ca isotope fractionation during calcite with an aqueous solution (Harrison et al. 2023), suggesting the effect of Ca isotope fraction on the rate determination can be neglected.

In addition, Fig. 4 showed fast calcite precipitation rates in Model C0 due to high HCO₃⁻ concentration. As a consequence, the Ca isotope ratio quickly approached a constant value during the first 5 days and remained constant at 0.208655, which is the same as the natural Ca isotope ratio. The results indicated that the labradorite dissolution and calcite precipitation are locked, and the rate ratio between labradorite and calcite is constant at 1.67. However, the temporal evolution of the Ca isotope ratio was measurable for Model D, because the variations of Ca isotope ratios were less due to the low calcite precipitation rates. Alternatively, the calcite precipitation rates and unidirectional labradorite dissolution rates could also be derived directly based on Ca isotope ratios instead of Si isotope ratios, which complements the measurement of unidirectional labradorite dissolution.

4.3 Local equilibrium vs. kinetics for calcite precipitation

The kinetics of calcite precipitation are significant for accurately illustrating the coupled dissolution and precipitation reaction system and predicting the mass of precipitation (Wolthers et al. 2012). Although different kinetic laws (TST and BCF) and local equilibrium were adopted for calcite, the amount of calcite precipitation and rates versus time at near-equilibrium didn't change, and the calcite saturation index remained constant for Model C and D series in Fig. 5a and b. This indicates that calcite precipitation was faster compared to labradorite dissolution and was not the rate-limited reaction in the reaction network. However, Fig. 5c showed the difference in the evolution of the isotope ratio was manifest enough for Model C with high HCO₃⁻, resulting from the minor difference of calcite precipitation rates between TST and BCF kinetic model and local equilibrium. There were two different modes of the evolution of Si and Ca isotope ratios, respectively. With redundant ²⁹Si and ⁴³Ca tracers and proper strength of spiking, distinguishing the differences in Model C0, C2 and C3 from an experimental perspective is feasible based on the measured Si and Ca isotope ratios.

Model D4 did not converge due to the low Ca concentration. Thus we just focused on Model C4 to explain the effect of the local equilibrium assumption for allophane and chalcedony. Assuming that the local equilibrium between the solution and allophane and chalcedony, Fig. 6a showed Si concentration increased sharply from 0.1 mM to 0.95 mM at the beginning. This was because the chalcedony seeds (1.0 mmol) dissolved to supply Si and maintained the equilibrium with respect to chalcedony. Therefore, the amount of chalcedony increased from 0.15 mmol, while the amount of allophane increased from 1.0 mmol, i.e., with 1.0 mmol allophane seeds. During the coupled reaction process, Si concentration kept constant, while Al concentration was almost zero during the period of the modeling, which illustrated that all Si and Al released from labradorite dissolution were immobilized through allophane and chalcedony precipitation.



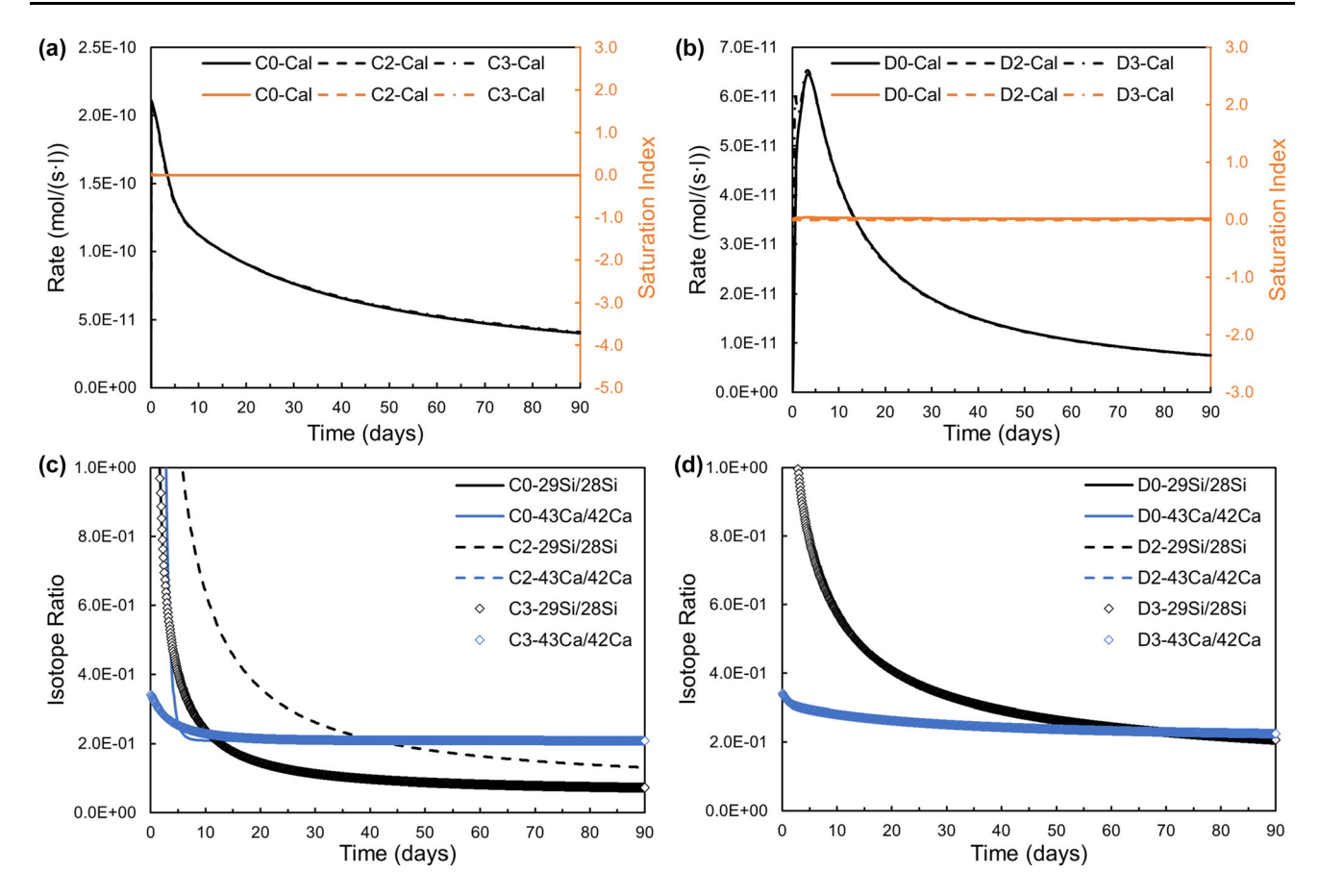


Fig. 5 Temporal evolution of calcite precipitation rates and isotope ratios using TST and BCF calcite precipitation kinetic models and the local equilibrium assumption in Model C and D series. Model C series (C0, C2 and C3): **a** precipitation rates and saturation index for calcite; **c** Isotope ratios of Si (29 Si)²⁸Si) and Ca (43 Ca)⁴²Ca). There are two different patterns for the evolution of Si and Ca isotope ratios, respectively. Model D series (D0, D2 and D3): **b** precipitation rates and saturation index for calcite; **d** Isotope ratios of Si (29 Si)²⁸Si) and Ca (43 Ca)⁴²Ca). The abbreviation of mineral names refers to Table 1

For Model C4, the SI of labradorite was always <-2 during 0–90 days, labradorite dissolved faster and more secondary minerals precipitated in Model C4 compared with Model C0, especially chalcedony (Fig. 6b and c). Calcite was always at near-equilibrium, and the labradorite dissolution and calcite precipitation were still locked, even if the local equilibrium between the solution and allophane and chalcedony was assumed. The evolution of Ca isotope ratio supported the above results (Fig. 6d). The results indicated that the mass transfer and reaction progress of the coupled system are affected by the local equilibrium of allophane and chalcedony, and the assumption can be tested following the experimental design through multi-isotope doped experiments.

5 Discussion

Our reaction path modeling shows that at 60 °C and after 5 days of reaction, the solution chemistry reached the near-equilibrium regime (Figs. 2 and 3) with respect to

labradorite. An order-of-magnitude reduction in dissolution rates from far-from-equilibrium to near-equilibrium at a pH of ~ 8.5 was observed between Model C0 and C1. The sharp decrease of dissolution rate may account for the one to two orders of magnitude discrepancy between previous laboratory determinations of feldspar dissolution rates (in highly undersaturated solutions) and field-based estimates (in solutions closer to equilibrium) (Zhu and Lu 2013).

Daval et al. (2010) carried out reaction path modeling to evaluate the effects of rate laws (Burch model vs TST rate laws) on diopside and labradorite dissolution and calcite precipitation (Daval et al. 2010). Using TST rate law in geochemical models would predict a dramatic overestimation of the carbonation rate than that using the r- ΔG_r relationship recommended by Taylor et al. (2000) and Daval et al. (2010) for labradorite and diopside, respectively. However, Carroll and Knauss (2005) did not observe such a mechanism switch in the labradorite dissolution experiments at 90 °C and pH \sim 3.2. The simulated temporal evolution of isotope ratios versus time (Figs. 2d and 3d) suggests that isotope doping is an



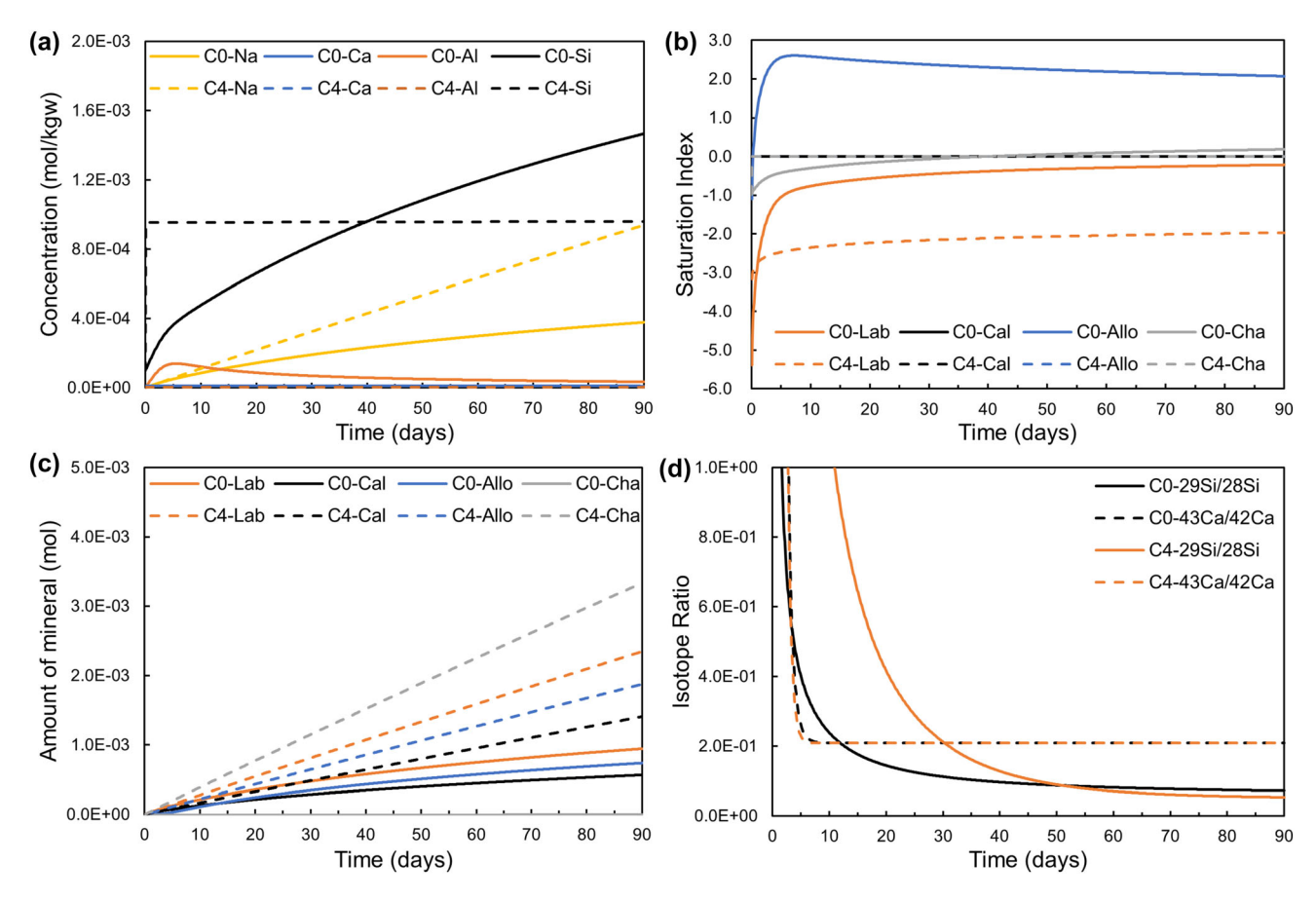


Fig. 6 Temporal evolution of the modeled systems with (Model C4) and without (Model C0) the assumption of allophane and chalcedony equilibrium. **a** Concentrations of aqueous species. **b** Saturation indexes of minerals. **c** Amount of mineral dissolution and precipitation. **d** Isotope ratios of Si (²⁹Si/²⁸Si) and Ca (⁴³Ca/⁴²Ca). The abbreviation of mineral names refers to Table 1

effective strategy to test whether labradorite dissolution follows TST or Burch-type rate law i.e., whether there is a dissolution mechanism switch. In our previous work, the unidirectional dissolution rates of albite based on the Si isotope doping suggest the mechanism switch from far-from-equilibrium to near-equilibrium did not occur under circum-neutral pH in low-temperature systems (Zhu et al. 2021).

In terms of calcite precipitation, the modeling results suggest we can derive calcite precipitation rates with multi-isotope doping at near-equilibrium. There is little difference between the results of TST and BCF kinetic model and the calcite local equilibrium model except for the isotope ratios (Fig. 5). An atomic force microscopic study under near-equilibrium conditions proposes that the calcite precipitation reaction occurs preferentially at the acute-acute kink sites and results in the inconsistencies in etch pit morphology, step anisotropy, and step activation energies with those of studies far-from-equilibrium (Xu et al. 2010). Other than instantaneous calcite growth on the calcite seeds, calcite also readily precipitates on the labradorite surfaces without inhibiting its dissolution (Stockmann et al.

2014), supporting ultramafic and basalt carbonation as a long-term carbon storage strategy.

6 Conclusions

In this study, we used geochemical modeling to aid the design of a series of isotope tracer-based labradorite dissolution experiments, which intend to decipher how labradorite dissolution and calcite and clayey minerals precipitation reactions are coupled. Geochemical modeling shows that the coupled system evolved from far-fromequilibrium to near-equilibrium conditions after a few days and maintained near-equilibrium until all labradorite was exhausted. The modeling results show that unidirectional labradorite dissolution rates can be obtained at various solution saturation states, which supports the determination of whether the dissolution mechanism of labradorite will change as the system moves from far from equilibrium to near equilibrium. Labradorite dissolution is coupled with calcite precipitation based on the Ca mass balance in the system. With multiple tracers (e.g., ⁴³Ca, ²⁹Si), we will also



be able to acquire calcite precipitation rates at near-equilibrium. It is inferred from our studies that the coupled system is labradorite dissolution controlled instead of calcite precipitation. In addition, labradorite dissolution rates are dependent on clay minerals (Si and Al) precipitation rates, which affects the coupled dissolution and precipitation process. These modeling results show the promise of implementing these multi-isotope doped experiments to understand the reaction kinetics of multiple mineral systems.

Acknowledgements CZ's research is partially supported by U.S. National Science Foundation grants EAR-2221907. Although the work was partly sponsored by agencies of the United States Government, the views and opinions of the authors expressed herein do not necessarily state or reflect those of the United States Government or any agency thereof. Financial support from Dalian University of Technology for MKC as a visiting Ph.D. student is also gratefully acknowledged.

Declarations

Conflict of interest The authors declare that there is no conflict of interest.

References

- Alekseyev VA, Medvedeva LS, Prisyagina NI, Meshalkin SS, Balabin AI (1997) Change in the dissolution rates of alkali feldspars as a result of secondary mineral precipitation and approach to equilibrium. Geochim Cosmochim Acta 61:1125–1142. https://doi.org/10.1016/S0016-7037(96)00405-X
- Berglund M, Wieser ME (2011) Isotopic compositions of the elements 2009 (IUPAC Technical Report). Pure Appl Chem 83(2):397–410. https://doi.org/10.1351/PAC-REP-10-06-02
- Black JR, Carroll SA, Haese RR (2015) Rates of mineral dissolution under CO₂ storage conditions. Chem Geol 399:134–144. https:// doi.org/10.1016/j.chemgeo.2014.09.020
- Brunauer S, Emmett PH, Teller E (1938) Adsorption of gases in multimolecular layers. J Am Chem Soc 60(2):309–319. https://doi.org/10.1021/ja01269a023
- Burch TE, Nagy KL, Lasaga AC (1993) Free energy dependence of albite dissolution kinetics at 80°C and pH 8.8. Chem Geol 105(1):137–162. https://doi.org/10.1016/0009-2541(93)90123-Z
- Burton WK, Cabrera N, Frank FC, Mott NF (1951) The growth of crystals and the equilibrium structure of their surfaces. Philos Trans R Soci London Ser a, Math Phys Sci 243(866):299–358. https://doi.org/10.1098/rsta.1951.0006
- Carroll SA, Knauss KG (2005) Dependence of labradorite dissolution kinetics on CO₂(aq), Al(aq), and temperature. Chem Geol 217(3):213–225. https://doi.org/10.1016/j.chemgeo.2004.12.008
- Chen M, Zhang Y, Liu S, Zhao C, Dong S, Song Y (2023) CO₂ transport and carbonate precipitation in the coupled diffusion-reaction process during CO₂ storage. Fuel 334:126805. https://doi.org/10.1016/j.fuel.2022.126805
- Dai ZX, Xu LL, Xiao T, McPherson B, Zhang XY, Zheng LG, Dong SN, Yang ZJ, Soltanian MR, Yang CB, Ampomah W, Jia W, Yin SX, Xu TF, Bacon D, Viswanathan H (2020) Reactive chemical transport simulations of geologic carbon sequestration: methods and applications. Earth Sci Rev 208:103265. https://doi.org/10.1016/j.earscirev.2020.103265

- Daval D, Hellmann R, Corvisier J, Tisserand D, Martinez I, Guyot F (2010) Dissolution kinetics of diopside as a function of solution saturation state: macroscopic measurements and implications for modeling of geological storage of CO₂. Geochim Cosmochim Acta 74(9):2615–2633. https://doi.org/10.1016/j.gca.2010.02.003
- Drever JI (1997) The geochemistry of natural waters: surface and groundwater environment, 3rd edn. Prentice-Hall, Englewood Cliffs, New Jersey
- Fu Q, Lu P, Konishi H, Dilmore R, Xu H, Seyfried WE, Zhu C (2009) Coupled alkali-feldspar dissolution and secondary mineral precipitation in batch systems: 1. New experiments at 200 °C and 300 bars. Chem Geol 258(3):125–135. https://doi.org/10. 1016/j.chemgeo.2008.09.014
- Gadikota G, Matter J, Kelemen P, Brady PV, Park A-HA (2020) Elucidating the differences in the carbon mineralization behaviors of calcium and magnesium bearing alumino-silicates and magnesium silicates for CO₂ storage. Fuel 277:117900. https://doi.org/10.1016/j.fuel.2020.117900
- Galeczka IM, Stefánsson A, Kleine BI, Gunnarsson-Robin J, Snæbjörnsdóttir SÓ, Sigfússon B, Gunnarsdóttir SH, Weisenberger TB, Oelkers EH (2022) A pre-injection assessment of CO₂ and H₂S mineralization reactions at the Nesjavellir (Iceland) geothermal storage site. Int J Greenh Gas Control 115:103610. https://doi.org/10.1016/j.ijggc.2022.103610
- Georg RB, Reynolds BC, Frank M, Halliday AN (2006) New sample preparation techniques for the determination of Si isotopic compositions using MC-ICPMS. Chem Geol 235(1):95–104. https://doi.org/10.1016/j.chemgeo.2006.06.006
- Gudbrandsson S, Wolff-Boenisch D, Gislason SR, Oelkers EH (2011) An experimental study of crystalline basalt dissolution from 2 ≤ pH ≤ 11 and temperatures from 5 to 75 °C. Geochim Cosmochim Acta 75(19):5496–5509. https://doi.org/10.1016/j.gca.2011.06.035
- Gysi AP, Stefánsson A (2012) Experiments and geochemical modeling of CO₂ sequestration during hydrothermal basalt alteration. Chem Geol 306–307:10–28. https://doi.org/10.1016/j.chemgeo.2012.02.016
- Harrison AL, Heuser A, Liebetrau V, Eisenhauer A, Schott J, Mavromatis V (2023) Equilibrium Ca isotope fractionation and the rates of isotope exchange in the calcite-fluid and aragonitefluid systems at 25 °C. Earth Plan Sci Lett 603:117985. https:// doi.org/10.1016/j.epsl.2022.117985
- Helgeson HC, Murphy WM, Aagaard P (1984) Thermodynamic and kinetic constraints on reaction rates among minerals and aqueous solutions. II. Rate constants, effective surface area, and the hydrolysis of feldspar. Geochim Cosmochim Acta 48(12):2405–2432. https://doi.org/10.1016/0016-7037(84)90294-1
- Hellmann R, Tisserand D (2006) Dissolution kinetics as a function of the Gibbs free energy of reaction: an experimental study based on albite feldspar. Geochim Cosmochim Acta 70(2):364–383. https://doi.org/10.1016/j.gca.2005.10.007
- Heřmanská M, Voigt MJ, Marieni C, Declercq J, Oelkers EH (2022)
 A comprehensive and internally consistent mineral dissolution rate database: Part I: primary silicate minerals and glasses. Chem Geol 597:120807. https://doi.org/10.1016/j.chemgeo.2022.120807
- Heřmanská M, Voigt MJ, Marieni C, Declercq J, Oelkers EH (2023) A comprehensive and consistent mineral dissolution rate database: part II: secondary silicate minerals. Chem Geol. https://doi.org/10.1016/j.chemgeo.2023.121632
- Lagache M (1976) New data on the kinetics of the dissolution of alkali feldspars at 200°C in CO₂ charged water. Geochim Cosmochim Acta 40:157–161. https://doi.org/10.1016/0016-7037(76)90173-3



- Lasaga AC (1998) Kinetic theory in the earth sciences, 1st edn. Princeton University Press, Princeton, New Jersey
- Lasaga AC (1981) Chapter 4. Transition state theory. In: Lasaga AC, Kirkpatrick J (Eds.) Book. De Gruyter, pp 135–170. https://doi. org/10.1515/9781501508233-008
- Li L, Maher K, Navarre-Sitchler A, Druhan J, Meile C, Lawrence C, Moore J, Perdrial J, Sullivan P, Thompson A, Jin L, Bolton EW, Brantley SL, Dietrich WE, Mayer KU, Steefel CI, Valocchi A, Zachara J, Kocar B, McIntosh J, Tutolo BM, Kumar M, Sonnenthal E, Bao C, Beisman J (2017) Expanding the role of reactive transport models in critical zone processes. Earth Sci Rev 165:280–301. https://doi.org/10.1016/j.earscirev.2016.09. 001
- Liu F, Lu P, Zhu C, Xiao Y (2011) Coupled reactive flow and transport modeling of CO₂ sequestration in the Mt. Simon sandstone formation, Midwest U.S.A. Int J Greenh Gas Control 5(2):294–307. https://doi.org/10.1016/j.ijggc.2010.08.008
- Liu Z, Rimstidt JD, Zhang Y, Yuan H, Zhu C (2016) A stable isotope doping method to test the range of applicability of detailed balance. Geochem Perspect Lett 2:78–86. https://doi.org/10. 7185/geochemlet.1608
- Lu P, Konishi H, Oelkers E, Zhu C (2015) Coupled alkali feldspar dissolution and secondary mineral precipitation in batch systems: 5. Results of K-feldspar hydrolysis experiments. Chin J Geochem 34(1):1–12. https://doi.org/10.1007/s11631-014-0029-z
- Lu P, Zhang G, Huang Y, Apps J, Zhu C (2022) Dawsonite as a temporary but effective sink for geological carbon storage. Int J Greenh Gas Control 119:103733. https://doi.org/10.1016/j.ijggc. 2022.103733
- Maher K, Steefel CI, White AF, Stonestrom DA (2009) The role of reaction affinity and secondary mienrals in regulating chemical weathering rates at the Santa Cruz Soil Chronosequence. California Geochim Cosmochim Acta 73(10):2804–2831. https://doi.org/10.1016/j.gca.2009.01.030
- Marini L (2007) Geological sequestration of carbon dioxide: thermodynamics, kinetics, and reaction path modeling. Elsevier, Heidelberg
- Marty NCM, Claret F, Lassin A, Tremosa J, Blanc P, Made B, Giffaut E, Cochepin B, Tournassat C (2015) A database of dissolution and precipitation rates for clay-rocks minerals. Appl Geochem 55:108–118. https://doi.org/10.1016/j.apgeochem.2014.10.012
- Ohlin CA, Villa EM, Rustad JR, Casey WH (2009) Dissolution of insulating oxide materials at the molecular scale. Nat Mater 9:11. https://doi.org/10.1038/nmat2585
- Palandri J, Kharaka Y (2004) A compilation of rate parameters of water-mineral interaction kinetics for application to geochemical modeling. Open-File Rep, 70
- Parkhurst DL, Appelo C (2013) Description of input and examples for PHREEQC version 3—a computer program for speciation, batch-reaction, one-dimensional transport, and inverse geochemical calculations. US Geol Surv Tech Methods 6:497
- Pham VTH, Lu P, Aagaard P, Zhu C, Hellevang H (2011) On the potential of CO₂—water—rock interactions for CO₂ storage using a modified kinetic model. Int J Greenh Gas Control 5(4):1002–1015. https://doi.org/10.1016/j.ijggc.2010.12.002
- Ralston SJ (2018) Dissolution rates of allophane, Fe-allophane, and hisingerite and implications for aqueous alteration on mars and in potential returned martian samples. Dissertation, University of Nevada, Las Vegas
- Raza A, Glatz G, Gholami R, Mahmoud M, Alafnan S (2022) Carbon mineralization and geological storage of CO₂ in basalt: mechanisms and technical challenges. Earth Sci Rev 229:104036. https://doi.org/10.1016/j.earscirev.2022.104036
- Rimstidt JD (2014) Geochemical rate models: an introduction to geochemical kinetics. Cambridge University Press, Cambridge. https://doi.org/10.1017/CBO9781139342773

- Schott J, Pokrovsky OS, Oelkers EH (2009) The link between mineral dissolution/precipitation kinetics and solution chemistry. Rev Mineral Geochem 70(1):207–258. https://doi.org/10.2138/rmg. 2009.70.6
- Snæbjörnsdóttir SÓ, Oelkers EH, Mesfin K, Aradóttir ES, Dideriksen K, Gunnarsson I, Gunnlaugsson E, Matter JM, Stute M, Gislason SR (2017) The chemistry and saturation states of subsurface fluids during the in situ mineralisation of CO₂ and H₂S at the CarbFix site in SW-Iceland. Int J Greenh Gas Control 58:87–102. https://doi.org/10.1016/j.ijggc.2017.01.007
- Snæbjörnsdóttir SÓ, Gislason SR, Galeczka IM, Oelkers EH (2018) Reaction path modelling of in-situ mineralisation of CO₂ at the CarbFix site at Hellisheidi, SW-Iceland. Geochim Cosmochim Acta 220:348–366. https://doi.org/10.1016/j.gca.2017.09.053
- Steefel CI, MacQuarrie KTB (1996) Approaches to modeling of reactive transport in porous media. Rev Mineral Geochem 34(1):85–129
- Steefel CI, Appelo CAJ, Arora B, Jacques D, Kalbacher T, Kolditz O, Lagneau V, Lichtner PC, Mayer KU, Meeussen JCL, Molins S, Moulton D, Shao H, Simunek J, Spycher N, Yabusaki SB, Yeh GT (2015) Reactive transport codes for subsurface environmental simulation. Comput Geosci 19(3):445–478. https://doi.org/10.1007/s10596-014-9443-x
- Stockmann GJ, Wolff-Boenisch D, Bovet N, Gislason SR, Oelkers EH (2014) The role of silicate surfaces on calcite precipitation kinetics. Geochim Cosmochim Acta 135:231–250. https://doi.org/10.1016/j.gca.2014.03.015
- Stumm W (1992) Chemistry of solid-water interfaces: processes at the mineral-water and particle-water interface in natural systems, 1st edn. John Wiley & Sons, New York
- Taylor AS, Blum JD, Lasaga AC (2000) The dependence of labradorite dissolution and Sr isotope release rates on solution saturation state. Geochim Cosmochim Acta 64(14):2389–2400. https://doi.org/10.1016/S0016-7037(00)00361-6
- Thommes M, Kaneko K, Neimark AV, Olivier JP, Rodriguez-Reinoso F, Rouquerol J, Sing KSW (2015) Physisorption of gases, with special reference to the evaluation of surface area and pore size distribution (IUPAC Technical Report). Pure Appl Chem 87:1051–1069
- Wolff-Boenisch D, Wenau S, Gislason SR, Oelkers EH (2011) Dissolution of basalts and peridotite in seawater, in the presence of ligands, and CO₂: implications for mineral sequestration of carbon dioxide. Geochim Cosmochim Acta 75(19):5510–5525. https://doi.org/10.1016/j.gca.2011.07.004
- Wolthers M, Nehrke G, Gustafsson JP, Van Cappellen P (2012) Calcite growth kinetics: modeling the effect of solution stoichiometry. Geochim Cosmochim Acta 77:121–134. https:// doi.org/10.1016/j.gca.2011.11.003
- Xiong W, Giammar D (2014) Forsterite carbonation in zones with transport limited by diffusion. Environ Sci Technol Lett 1(8):333–338. https://doi.org/10.1021/ez500182s
- Xu M, Hu X, Knauss KG, Higgins SR (2010) Dissolution kinetics of calcite at 50–70°C: an atomic force microscopic study under near-equilibrium conditions. Geochim Cosmochim Acta 74(15):4285–4297. https://doi.org/10.1016/j.gca.2010.04.066
- Zhang G, Lu P, Wei X, Zhu C (2016) Impacts of mineral reaction kinetics and regional groundwater flow on long-term CO₂ fate at sleipner. Energ Fuel 30(5):4159–4180. https://doi.org/10.1021/acs.energyfuels.5b02556
- Zhang YL, Hu B, Teng YG, Tu K, Zhu C (2019) A library of BASIC scripts of reaction rates for geochemical modeling using PHREEQC. Comput Geosci 133:104316. https://doi.org/10.1016/j.cageo.2019.104316
- Zhu C (2005) In situ feldspar dissolution rates in an aquifer. Geochim Cosmochim Acta 69(6):1435–1453. https://doi.org/10.1016/j. gca.2004.09.005



- Zhu C (2009) Geochemical modeling of reaction paths and geochemical reaction networks. Rev Mineral Geochem 70(1):533–569. https://doi.org/10.2138/rmg.2009.70.12
- Zhu C, Lu P (2013) The coupling of dissolution and precipitation reactions as the main contributor to the apparent field-lab rate discrepancy. Proc Earth Planet Sci 7:948–952. https://doi.org/10.1016/j.proeps.2013.03.051
- Zhu C, Liu Z, Zhang Y, Wang C, Scheafer A, Lu P, Zhang G, Georg RB, Yuan H-l, Rimstidt JD (2016) Measuring silicate mineral dissolution rates using Si isotope doping. Chem Geol 445:146–163. https://doi.org/10.1016/j.chemgeo.2016.02.027
- Zhu C, Donald Rimstidt J, Zhang Y, Kang J, Schott J, Yuan H (2020) Decoupling feldspar dissolution and precipitation rates at nearequilibrium with Si isotope tracers: implications for modeling silicate weathering. Geochim Cosmochim Acta 271:132–153. https://doi.org/10.1016/j.gca.2019.12.024
- Zhu C, Zhang Y, Rimstidt JD, Gong L, Burkhart JAC, Chen K, Yuan H (2021) Testing hypotheses of albite dissolution mechanisms at near-equilibrium using Si isotope tracers. Geochim Cosmochim Acta 303:15–37. https://doi.org/10.1016/j.gca.2021.03.023
- Zhu C, Blum AE, Veblen DR (2004) Feldspar dissolution rates and clay precipitation in the Navajo aquifer at Black Mesa, Arizona, USA. In: Wanty RB, Seal RRI (Eds) Water-Rock Interaction 11.
 A. A. Balkema, Saratoga, New York, 895–899

Springer Nature or its licensor (e.g. a society or other partner) holds exclusive rights to this article under a publishing agreement with the author(s) or other rightsholder(s); author self-archiving of the accepted manuscript version of this article is solely governed by the terms of such publishing agreement and applicable law.

